Chinese Chemical Letters 32 (2021) 2474–2478

Contents lists available at ScienceDirect

Chinese Chemical Letters

journal homepage: www.elsevier.com/locate/cclet

Communication

# Ultrathin zinc selenide nanosheet-based intercalation hybrid coupled with CdSe quantum dots showing enhanced photocatalytic $CO_2$ reduction

Zejun Zhao[a,1], Zailun Liu[b,c,1], Zhixiao Zhu[a], Fang Wang[a], Fei Teng[c], Wenjun Jiang[b,*], Yong Yang[a,*]

[a] State Key Laboratory of Solidification Processing, Center of Advanced Lubrication and Seal Materials, Northwestern Polytechnical University, Xi'an 710072, China
[b] Qian Xuesen Laboratory of Space Technology, China Academy of Space Technology, Beijing 100094, China
[c] School of Environmental Science and Engineering, Nanjing University of Information Science & Technology, Nanjing 210044, China

ARTICLE INFO

*Article history:*
Received 2 December 2020
Received in revised form 27 December 2020
Accepted 28 December 2020
Available online 13 January 2021

*Keywords:*
Inorganic-organic hybrid
ZnSe intercalation hybrid
CdSe quantum dots
Light absorption
Photocatalytic $CO_2$ reduction

ABSTRACT

Fabrication of well-designed heterojunctions is an extraordinarily attractive pathway for boosting the photocatalytic activity toward $CO_2$ photoreduction. Herein, a novel kind of nanosheet-based intercalation hybrid coupled with CdSe quantum dots (QDs) was successfully fabricated by a facile solvothermal method and served as photocatalyst for full-spectrum-light-driven $CO_2$ reduction. Ultra-small CdSe QDs were rationally *in-situ* introduced and coupled with lamellar ZnSe-intercalation hybrid nanosheet, resulting in the formation of CdSe QDs/ZnSe hybrid heterojunction. Significantly, the concentration of $Cd^{2+}$ could change directly the crystallinity and micromorphology of ZnSe intercalation hybrid, which in turn would impact on the photocatalysis activity. The optimized CdSe QDs/ZnSe hybrid-5 composite demonstrated a considerable CO yield rate of the 25.6 μmol $g^{-1}$ $h^{-1}$ without any additional cocatalysts or sacrificial agents assisting, making it one of the best reported performance toward $CO_2$ photoreduction under full-spectrum light. The elevated $CO_2$ photoreduction activity could be attributed to the special surface heterojunction, leading to improving the ability of light absorption and promoting the separation/transfer of photogenerated carriers. This present study developed a new strategy for designing inorganic-organic heterojunctions with enhanced photocatalyst for $CO_2$ photoreduction and provided an available way to simultaneously mitigate the greenhouse effect and alleviate energy shortage pressure.



The aggravation of greenhouse effect and the shortage of fossil fuels have drawn significant research attention for the purpose of exploring a feasible way to resolve both of them simultaneously [1–5]. Solar energy, as one of the most widely distributed energy resources, has been considered as an ideal clean energy due to its sustainable and inexhaustible supply [6–8]. In recent years, the boom of photocatalysis technology provides a feasible strategy to make full use of solar energy [9–12]. Among them, photocatalytic $CO_2$ reduction to CO have been regarded as one of the most promising strategies to realize the resource conversion [13–16]. The efficiency of photoreduction $CO_2$ usually depended on the performance of photocatalyst, involving the excitation of photogenerated carriers [17,18], migration and separation of charges as well as photocatalytic reaction on the catalytic surface [19,20]. For past decades, various catalysts for photoreduction $CO_2$ have been developed [21,22], but these catalysts usually suffered from some deficiencies such as inappropriate bandgap or band edge positions, unsatisfactory light response and rapid charge recombination, which was far from the demand to meet the practical applications [23–25]. Therefore, it is necessary to develop a new type of catalyst with excellent photocatalytic activity for $CO_2$ reduction [26].

Cadmium selenide (CdSe) with excellent visible-light responsivity [27], tunable energy band gap from 1.8 eV to 3.0 eV and sufficient conduction band (CB) potential well above the $H_2$ production potential (−0.41 eV *vs.* normal hydrogen electrode (NHE), pH 7) has been demonstrated exceptional catalytic activity

* Corresponding authors.
*E-mail addresses:* jiangwenjun@qxslab.cn (W. Jiang), yongyangfj@nwpu.edu.cn (Y. Yang).
[1] These authors contributed equally to this work.

https://doi.org/10.1016/j.cclet.2021.01.004

for efficient $CO_2$ reduction [28–31]. However, serious light corrosion and inferior stability decrease the efficiency of photocatalytic $CO_2$ reduction [32,33]. Various methods have been proposed to enhance the photocatalytic performance, such as synthesis of quantum dots, regulating the morphology and construction of heterojunction [34–36]. Recently, inorganic-organic hybrid II-VI semiconductors assembled with inorganic substance (MQ, M = Zn or Cd, Q = S or Se) and organic molecule (diethylenetriamine, amine) have demonstrated enhanced properties including electronic transport, optical response and band structures, which have attracted extensive potential application in photoelectric energy conversion [37–41]. It was indicated that sub-nanometer-scale periodic structures could induce strong quantum confinement effects, which could be used as functional parts or building blocks in various nanodevices [42,43]. For instance, the ZnS-DETA/CdS hierarchical hybrids exhibited efficient catalytic activity for $CO_2$ reduction owing to their unique features of visible light harvesting, high surface area and abundant catalytic active sites for adsorption and surface redox catalysis, promoting separation and transfer of photo-induced charge carriers [44]. In this regard, construction of the metal-chalcogenides semiconductors inorganic/organic-hybrid heterostructures and quantization strategy had been deemed as a simple and effective way to improve photocatalytic activity and stability through tuning the band structures of two different semiconductors [45–48].

In this work, CdSe quantum dots (QDs) attached to lamellar ZnSe intercalation hybrid labeled as CdSe QDs/ZnSe hybrid was successfully prepared by a simple solvothermal method and employed as catalyst for $CO_2$ photoreduction. The concentration of cadmium ions not only changed the crystal structure of products, but also had significant impacts on catalytic activity for $CO_2$ photoreduction. In this work, the moderate amounts of CdSe QDs can offer abundant active sites for $CO_2$ reduction and improve the absorption of solar energy efficiently. As a result, ZnSe intercalation hybrid was conducive to improving the absorption of $CO_2$ on catalyst surface. Compared with the ZnSe-intercalation hybrid, the optimized sample CdSe QDs/ZnSe hybrid-5 exhibited superior catalytic activity toward photocatalytic $CO_2$ reduction to CO under full-spectrum-light irradiation. Enhanced performance could be attributed to the unique heterojunction between ZnSe intercalation hybrid and ultra-small CdSe QDs, which could improve the abilities of light absorption and the separation/transfer of photogenerated carriers.

Fig. 1a shows the synthetic process of CdSe QDs/ZnSe hybrid composite. ZnSe-intercalation hybrid with a lamellar structure was initially obtained through a self-assembly process under the ligation and structure guiding functions of octylamine, resulting in the formation of inorganic-organic intercalation compounds. CdSe QDs coupled with ZnSe-intercalation hybrid was rationally fabricated in the same way when $Cd^{2+}$ was involved. Under the reaction procedure, CdSe QDs would be formed spontaneously and simultaneously coupled with lamellar ZnSe-intercalation hybrid, leading to the formation of CdSe QDs/ZnSe hybrid.

The micromorphology of ZnSe-intercalation hybrid was firstly investigated by scanning electron microscopy (SEM). Fig. S1a (Supporting information) clearly reveals that ZnSe-intercalation hybrid is composed of ultra-thin nanosheets displaying a flower-like structure. Transmission electron microscopy (TEM) image of ZnSe-intercalation hybrid shown in Fig. 1b indicates that numerous ultra-thin nanosheets were assembled together forming the ZnSe-intercalation hybrid. High-resolution transmission electronic microscopy (HRTEM) images clearly illustrate that the ultra-thin nanosheets have a periodic lamellar structure and the interlayer distance is up to 0.95 nm (Fig. 1c and Fig. S1b in Supporting information). Low-angle XRD test from 2° to 9.5° was conducted to analyze the lamellar structure of ZnSe-intercalation hybrid. Three

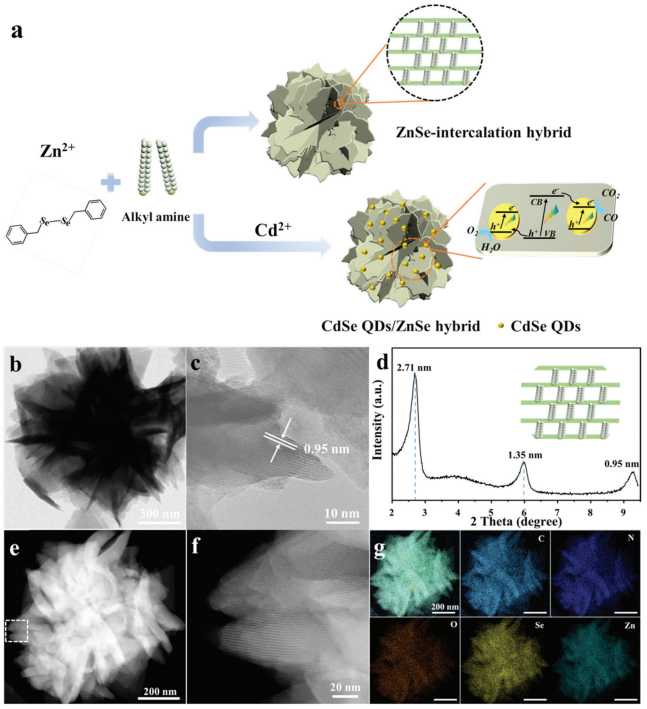


**Fig. 1.** (a) Synthesis process of the ZnSe-intercalation hybrid and CdSe QDs/ZnSe hybrid and their applications for photocatalysts $CO_2$ reduction. (b) TEM image of ZnSe-intercalation hybrid. (c) HRTEM image of ZnSe-intercalation hybrid. (d) Low-angle XRD pattern of ZnSe-intercalation hybrid from 2° to 9.5°. (e, f) HAADF-STEM image of ZnSe-intercalation hybrid. (g) EDS mapping images of ZnSe-intercalation hybrid.

diffraction peaks appeared at 3.25°, 6.50° and 9.28° in the low-angle XRD patterns reveal well-defined ZnSe-intercalation structure with interlayer distance, indicating the formation of amine intercalated ZnSe hybrid (Fig. 1d) [49]. These three peaks were corresponding to different interlamellar spacing of 2.71 nm, 1.35 nm and 0.95 nm, respectively. The low-angle XRD results are consistent with those of transmission analysis. High-angle annular dark-field scanning transmission electron microscopy (HAADF-STEM) image shown in Fig. S2a (Supporting information) further reveals that of ZnSe-intercalation hybrid nanosheets consist of single layer or multi-layer nanosheets. HRTEM image and the associated selected area electron diffraction (SAED) pattern (inset of Fig. S2b in Supporting information) show that ZnSe-intercalation hybrid possesses a lower crystallinity. In order to shed light on the phase composition of ZnSe-intercalation hybrid, XRD tests from 10° to 80° was further carried out. The characteristic peaks are corresponding to the ZnSe hexagonal phase but with a slight shift (Fig. S3a in Supporting information). The energy-dispersive X-ray (EDX) spectrum of ZnSe-intercalation hybrid shown in Fig. S3b (Supporting information) illustrates that ZnSe-intercalation hybrid was mainly composed of Zn, Se and C elements. HAADF-STEM image shown in Fig. 1e further illustrates that ZnSe-intercalation hybrid is assembled by the ultra-thin inorganic-organic intercalation nanosheets. High magnification HAADF-STEM image demonstrates that ZnSe-intercalation hybrid possesses a layered structure similar to periodic arrangement crystal (Fig. 1f). The EDS elemental mapping images of ZnSe-intercalation hybrid distinctly manifest the uniform distribution of elements throughout the whole structure, including Zn, Se, C, N and O elements (Fig. 1g). Corresponding EDS linear scanning elemental mapping images shown in Fig. S4 (Supporting information) also testify the elements distribution state. Through the above analysis, ZnSe-intercalation hybrid with a lamellar crystal

feature have been fabricated through structure-oriented function of octylamine during solvothermal reaction.

Subsequently, CdSe QDs/ZnSe hybrids were rationally designed and fabricated by adding a certain amount of cadmium acetate (5.0 mg and 10.0 mg) into the reaction system. As-obtained products were labeled as CdSe QDs/ZnSe hybrid-5, CdSe QDs/ZnSe hybrid-10, respectively. SEM images of CdSe QDs/ZnSe hybrid-5 are presented in Fig. 2a and Fig. S5a (Supporting information), in comparison with the ZnSe-intercalation hybrid, the morphology of CdSe QDs/ZnSe hybrid-5 has no distinct changes and still retains the flower-like structure. Fig. S5b (Supporting information) shows that CdSe QDs/ZnSe hybrid-5 is also constructed with the nanosheets. Many quantum dots marked with the small white circles are easily detected on the surface of nanosheets (Fig. 2b and Fig. S6 in Supporting information). And the diameter of CdSe QDs is about 1–2 nm (Fig. S7 in Supporting information). The interplanar distance about 0.22 nm is corresponded to the (110) crystal plane of CdSe (Fig. 2c and Fig. S8 in Supporting information). We proposed that cadmium ions preferred to form CdSe crystal rather than assemble into the inorganic-organic intercalation composites. As presented in Fig. 2d, HAADF-STEM image distinctly shows that CdSe QDs/ZnSe hybrid-5 is constructed by the ultra-thin nanosheets, resulting the flower like construction. Further careful observation of the HAADF-STEM image of CdSe QDs/ZnSe hybrid-5 exhibited in Fig. 2e, periodic layered structure of ultra-thin nanosheets have not been transformed. EDS elemental mapping images shown in Fig. 2f verify the uniform distribution of elements Cd, C, N, Se and Zn, indicating that CdSe QDs was incorporated in CdSe QDs/ZnSe hybrid-5.

It was noteworthy that $Cd^{2+}$ had significant influence on the crystallinity and micromorphology of products. The effects of $Cd^{2+}$ on the layered structure of ZnSe-intercalation hybrid were investigated in detailed. Low-angle XRD patterns show that the intensity of diffraction peaks at 3.25°, 6.50° and 9.28° decrease gradually with the increase of $Cd^{2+}$ concentration (Fig. 3a). The diffraction peaks had completely disappeared when 20 mg cadmium acetate was involved (Fig. S9 in Supporting information). CdSe QDs would be produced when $Cd^{2+}$ was introduced, which could influence the formation of layered ZnSe-intercalation hybrid. With the increase of $Cd^{2+}$ concentration, the crystallization effects of cadmium ions became more significant than self-assembly effects. Besides, the crystallization characteristics of the samples would also be affected by the concentration of $Cd^{2+}$. Fig. 3b shows that the intensity of diffraction patterns exhibiting a decreasing trend with the increase of $Cd^{2+}$ concentration. As for CdSe QDs/ZnSe hybrid-10, only two broad peaks can be found in the diffraction patterns, which indicates that the addition of $Cd^{2+}$ will

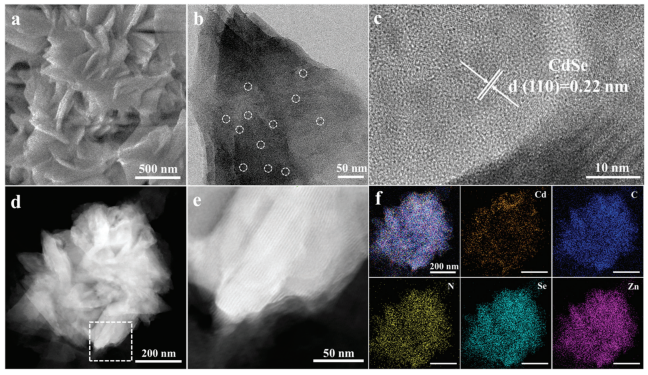


**Fig. 2.** (a) SEM image of CdSe QDs/ZnSe hybrid-5. (b) TEM image of CdSe QDs/ZnSe hybrid-5. (c) HRTEM image CdSe QDs/ZnSe hybrid-5. (d, e) HAADF-STEM image of CdSe QDs/ZnSe hybrid-5. (f) EDS mapping images of CdSe QDs/ZnSe hybrid-5.

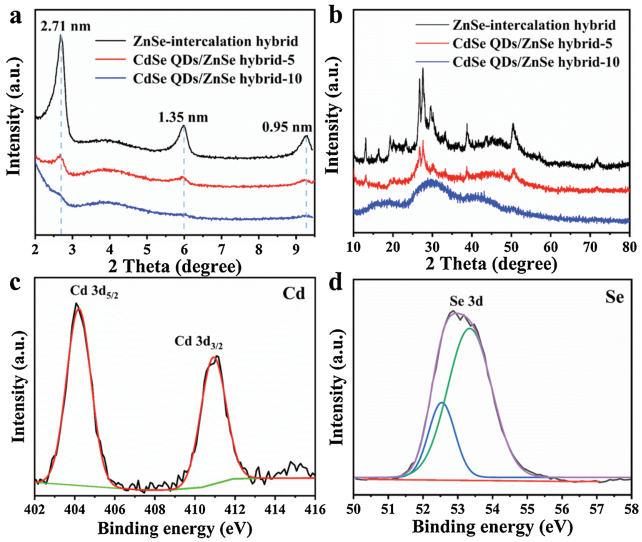


**Fig. 3.** (a) Low-angle XRD patterns from 2° to 9.5°. (b) XRD patterns from 10° to 80°. High-resolution XPS spectra: (c) Cd 3d and (d) Se 3d.

disturb the crystallization of ZnSe-intercalation hybrid even at lower variation level of concentration. Interestingly, after coupling with CdSe QDs, but there were no diffraction peaks about CdSe found suggesting that either the content of CdSe QDs was very low or the crystalline size of CdSe QDs was too small beyond the sensitivity of XRD. The TEM image of CdSe QDs/ZnSe hybrid-10 in Fig. S10 (Supporting information) shows the morphology of CdSe QDs/ZnSe hybrid-10 have changed dramatically: the arrangement of superlattice structure disappears gradually with the increasing of $Cd^{2+}$ concentration. Similar transformation can be found in the TEM image of CdSe QDs/ZnSe hybrid-20 (Fig. S11 in Supporting information). It could be concluded that the $Cd^{2+}$ would not only lead to the formation of CdSe QDs, but also influence the micromorphology of products.

The surface chemical compositions and their valence states were further analyzed by X-ray photoelectron spectroscopy (XPS). The XPS survey spectrum is shown in Fig. S12 (Supporting information), distinctly, signal peaks observed at around 53.16 eV (Se 3d), 285.0 eV (C 1s), 398.0 eV (N 1s), 530.54 eV (O 1s), 1021.36 eV (Zn 2p), respectively, demonstrate that ZnSe-intercalation hybrid is comprised of Se, C, N, O and Zn elements. Compared with the ZnSe-intercalation hybrid, the signal intensity of CdSe QDs/ZnSe hybrid-5 is higher than that of ZnSe-intercalation hybrid. In addition, the peak corresponding to Cd element can be detected in CdSe QDs/ZnSe hybrid-5 spectrum at 404.28 eV after cadmium ions are introduced confirming that Cd have been successful integrated into ZnSe-intercalation hybrid. High-resolution XPS spectrum of Cd 3d is shown in Fig. 3c, two peaks around 404.02 eV and 410.9 eV are observed in the Cd 3d spectrum, which are assigned to the Cd $3d_{5/2}$ and Cd $3d_{3/2}$, respectively. In Se 1s spectrum, two peaks located at 52.77 and 53.6 eV belong to the Se $3d_{5/2}$ and Se $3d_{3/2}$, respectively (Fig. 3d). In this regard, ultra-small CdSe QDs formed and simultaneously coupled with lamellar ZnSe-intercalation hybrid nanosheet, resulting in the formation of CdSe QDs/ZnSe hybrid heterojunction.

It is well known that the efficient light adsorption is one of the key requirements for photocatalyst [50,51]. In order to figure out the light adsorption performance of the samples, UV–vis diffuse reflectance spectra (UV-DRS) tests were implemented. Fig. 4a shows that the pure ZnSe-intercalation hybrid exhibits the absorption edge below 320 nm, which greatly limit the utilization

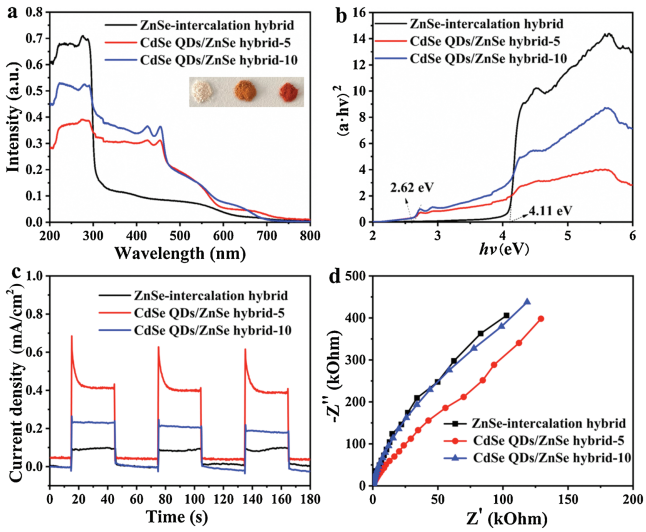


**Fig. 4.** (a) UV/vis diffuse reflectance spectra of the samples, insert shows the samples photo from left to right: ZnSe-intercalation hybrid, CdSe QDs/ZnSe hybrid-5, CdSe QDs/ZnSe hybrid-10, respectively. (b) Tauc plots of the samples. (c) Photocurrent response curves of the samples. (d) EIS Nyquist plots for the samples.

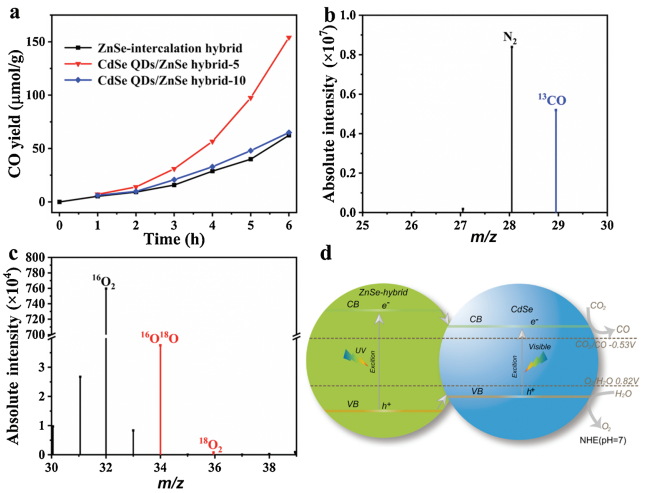


**Fig. 5.** (a) Time-yield plots of CO under irradiation of full-spectrum light. (b) GC–MS analysis of CO generated from the $^{13}CO_2$ isotope experiment over CdSe QDs/ZnSe hybrid-5 using $NaH^{13}CO_3$ as the source of $^{13}CO_2$. (c) GC–MS analysis of $O_2$ generated from the $H_2{}^{18}O$ isotope experiment over CdSe QDs/ZnSe hybrid-5 using $H_2{}^{18}O$ ($H_2{}^{16}O$:$H_2{}^{18}O$ = 1:1). (d) Possible reaction mechanism of photocatalytic $CO_2$ reduction for CdSe QDs/ZnSe hybrid-5.

of light. With the increasing Cd content, an absorption edge appears at 480 nm, which is attributed to CdSe QDs. Moreover, the adsorption band in 300−600 nm intensified, indicating that the CdSe QDs/ZnSe hybrid can increase the absorption range of light (Fig. S13 in Supporting information). The color of the samples inserted in Fig. 4a demonstrated that the color of the sample is influenced by the concentration of $Cd^{2+}$: with the increase of $Cd^{2+}$ concentration, the color changes from white to yellow and then to dark red. As displayed in Fig. 4b, the band gap of ZnSe-intercalation hybrid is calculated to be 4.11 eV, indicating that the ZnSe-intercalation hybrid need a higher energy of light to excite. Compared with ZnSe-intercalation hybrid, the CdSe QDs/ZnSe hybrid-5 and CdSe QDs/ZnSe hybrid-10 show another band gap at the 2.62 eV, which suggests the CdSe QDs/ZnSe hybrid heterojunction is successfully formed. The $N_2$ adsorption-desorption isotherms and the pore size distribution of the CdSe QDs/ZnSe hybrid-5 are shown in Fig. S14 (Supporting information). The Brunauer-Emmett-Teller (BET) specific surface area of the CdSe QDs/ZnSe hybrid-5 is 48.43 $m^2$/g and the pore structure is mainly microporous with a size range from 2 nm to 25 nm. The larger specific surface area and hierarchical pore distribution is favor of the $CO_2$ adsorption and improve the efficiency of photocatalysis.

To further investigate the photoreduction activity of CdSe QDs/ZnSe hybrid, the various photoelectrochemical characterizations were conducted to reveal the kinetics properties of photogenerated carriers. The photocurrent response measurements were performed to investigate the charge separation/transfer in as-prepared samples. The data in Fig. 4c demonstrate that the CdSe QDs/ZnSe hybrid-5 exhibits much larger current density than that of ZnSe-intercalation hybrid and CdSe QDs/ZnSe hybrid-10, suggesting enhanced electron and hole separation/transfer in CdSe QDs/ZnSe hybrid-5. The charge transfer resistance was investigated by electrochemical impedance spectroscopy (EIS). As shown in Fig. 4d, the diameter of the semicircle Nyquist plot for CdSe QDs/ZnSe hybrid-5 is smaller than that of ZnSe-intercalation hybrid and CdSe QDs/ZnSe hybrid-10, indicating a lower charge transfer resistance and more efficient photogenerated carriers transport in CdSe QDs/ZnSe hybrid-5.

The photocatalytic activities of the samples were evaluated by $CO_2$ photoreduction reaction under a 300 W Xe lamp irradiation (Fig. S15 in Supporting information). The gas phase products were identified and quantified by the gas chromatography, CO was the major phase products and no $H_2$ was detected during the $CO_2$ photoreduction process. In the absence of cocatalysts and sacrificial agents, the $CO_2$ photoreduction activity of ZnSe-intercalation hybrid and CdSe QDs/ZnSe hybrid samples are shown in Fig. 5a and Fig. S16 (Supporting information). At beginning, the CdSe QDs/ZnSe hybrids manifested unsatisfactory $CO_2$ photoreduction activity. When the cadmium acetate was up to 5 mg, the CdSe QDs/ZnSe hybrid-5 (25.6 μmol $g^{-1}$ $h^{-1}$) exhibited a 2.5 times enhanced $CO_2$ photoreduction activity comparing with ZnSe-intercalation hybrid (10.4 μmol $g^{-1}$ $h^{-1}$), which was presented in Fig. S17 (Supporting information). The catalytic activity of CdSe QDs/ZnSe hybrid-5 is superior to most of the previously reported photocatalysts (Table S1 in Supporting information). Enhanced $CO_2$ photoreduction activity of CdSe QDs/ZnSe hybrid-5 indicated that the CdSe/ZnSe heterojunction could increase the light absorption and promote the separation/transfer of photogenerated carriers.

In order to confirm the source of carbon, the $^{13}C$ isotopic labeling experiment was performed. As shown in Fig. 5b, the peak at $m/z$ = 29 ($^{13}CO$) indicated that the formation of CO is indeed derived from the reduction of $CO_2$. In addition, the $^{18}O$ isotopic labeling experiment was also carried out. It was noted that the peak at $m/z$ = 34 ($^{16}O^{18}O$) and $m/z$ = 38 ($^{18}O^{18}O$) can be observed, indicating that the formation of $O_2$ is indeed derived from the oxidation of water (Fig. 5c). Based on the results mentioned above, we proposed that the possible mechanism of photocatalytic $CO_2$ reduction in Fig. 5d. When light irradiated on the surface of CdSe/ZnSe, electron would be excited from the valence band to the conduction band, and leaving holes in the valence band. Then, under the effect of diffusion potential energy caused by the CdSe/ZnSe heterostructure type III band alignment, the electrons migrated to the CdSe conduction band, and the holes in the valence band of ZnSe also migrated to the CdSe valence band. As a result, the photogenerated carriers were well separated, reducing the recombination opportunity of photogenerated carriers. The photogenerated holes in CdSe valence band could oxidize into oxygen, and the electrons in the CdSe conduction band would react with $CO_2$ molecule into CO.

In summary, ultra-small CdSe QDs were rationally *in-situ* introduced and coupled with lamellar ZnSe-intercalation hybrid

nanosheet, resulting in the formation of CdSe QDs/ZnSe hybrid heterojunction. It was demonstrated that the optimized sample CdSe QDs/ZnSe hybrid-5 exhibited excellent $CO_2$ photoreduction activity: a considerable CO yield rate of 25.6 $\mu mol\ g^{-1}\ h^{-1}$ could be obtained in the absence of any extra cocatalysts or sacrificial agents under full-spectrum light irradiation, one of the best reported performance toward $CO_2$ photoreduction under full-spectrum light. It was proposed that CdSe QDs/ZnSe hybrid-5 heterojunction could increase the light absorption and promote the separation/transfer of photogenerated carriers, thus improving the performance of photocatalytic $CO_2$ reduction. This work might provide a new approach for designing CdSe QDs coupling ZnSe nanosheet-based intercalation hybrid for photocatalytic $CO_2$ reduction to CO.

## Declaration of competing interest

The authors report no declarations of interest.

## Acknowledgments

This work was supported by the National Natural Science Foundation of China (Nos. 51902266 and 22002185), the Fundamental Research Funds for the Central Universities (Nos. 310201QD0410 and 3102019ZD0403), the Natural Science Foundation of Beijing (No. 2204100) and Natural Science Foundation of Shaanxi (No. 2020JQ-143). The Project supported by the Research Fund of the State Key Laboratory of Solidification Processing (NPU), China (No. 2019-TS-12). We would like to thank the Analytical & Testing Center of Northwestern Polytechnical University for TEM characterizations.

## Appendix A. Supplementary data

Supplementary material related to this article can be found, in the online version, at doi:https://doi.org/10.1016/j.cclet.2021.01.004.

## References

[1] M. Zhou, S. Wang, P. Yang, C. Huang, X. Wang, ACS Catal. 8 (2018) 4928–4936.
[2] W. Zhong, R. Sa, L. Li, et al., J. Am. Chem. Soc. 141 (2019) 7615–7621.
[3] X. Shi, L. Qin, G. Xu, et al., Chem. Commun. 56 (2020) 3713–3716.
[4] Z. Zhao, Z. Zhu, H. Zhang, et al., Appl. Surf. Sci. 534 (2020) 147631.
[5] L. Wang, E. Guan, Y. Wang, et al., Nat. Commun. 11 (2020) 1033.
[6] Y. Yang, S. Wang, J. Zhang, et al., Inorg. Chem. Front. 2 (2015) 931–937.
[7] Y. Yu, J. Zhang, X. Wu, W. Zhao, B. Zhang, Angew. Chem. Int. Ed. 51 (2012) 897–900.
[8] H. Zhao, A. Vomiero, F. Rosei, Small 16 (2020) 2000804.
[9] Y. Yang, Y. Yang, S. Chen, et al., Nat. Commun. 8 (2017) 1559.
[10] Y. Wang, S. Wang, S.L. Zhang, X.W. Lou, Angew. Chem. Int. Ed. 59 (2020) 11918–11922.
[11] W. Weng, S. Wang, W. Xiao, X.W. Lou, Adv. Mater. 32 (2020) 2001560.
[12] S. Wang, B. Zhu, M. Liu, et al., Appl. Catal. B: Environ. 243 (2019) 19–26.
[13] W. Wang, D. Xu, B. Cheng, J. Yu, C. Jiang, J. Mater. Chem. A 5 (2017) 5020.
[14] S. Wang, B.Y. Guan, X.W. Lou, J. Am. Chem. Soc. 140 (2018) 5037–5040.
[15] R. Li, W. Zhang, K. Zhou, Adv. Mater. 30 (2018) 1705512.
[16] M. Liang, T. Borjigin, Y. Zhang, et al., Appl. Catal. B: Environ. 243 (2019) 566–575.
[17] H. Yu, E. Haviv, R. Neumann, Angew. Chem. Int. Ed. 59 (2020) 6219–6223.
[18] X. Ren, M. Gao, Y. Zhang, et al., Appl. Catal. B: Environ. 274 (2020) 119063.
[19] L. Qiao, M. Song, A. Geng, S. Yao, Chin. Chem. Lett. 30 (2019) 1273–1276.
[20] F. Mei, J. Zhang, K. Dai, G. Zhu, C. Liang, Dalton Trans. 48 (2019) 1067–1074.
[21] X.B. Li, C. H.Tung, L.Z. Wu, Angew. Chem. Int. Ed. 58 (2019) 10804–10811.
[22] P. Li, G. Luo, S. Zhu, et al., Appl. Catal. B: Environ. 274 (2020) 119115.
[23] A. Bafaqeer, M. Tahir, N.A.S. Amin, Appl. Catal. B: Environ. 242 (2019) 312–326.
[24] C. Bie, B. Zhu, F. Xu, L. Zhang, J. Yu, et al., Adv. Mater. 31 (2019) 1902868.
[25] Y. Chao, P. Zhou, N. Li, et al., Adv. Mater. 31 (2019) 1807226.
[26] S. Ji, Y. Qu, T. Wang, et al., Angew. Chem. Int. Ed. 59 (2020) 10651–10657.
[27] D. Zhong, W. Liu, P. Tan, et al., Appl. Catal. B: Environ. 227 (2018) 1–12.
[28] R. Shi, Y. Cao, Y. Bao, et al., Adv. Mater. 29 (2017) 1700803.
[29] W. Xia, J. Wu, J.C. Hu, et al., ChemSusChem 12 (2019) 4617–4622.
[30] H.L. Wu, X.B. Li, C.H. Tung, L.Z. Wu, Adv. Mater. 31 (2019) 1900709.
[31] F. Raziq, A. Hayat, M. Humayun, et al., Appl. Catal. B: Environ 270 (2020) 118867.
[32] F. He, B. Zhu, B. Cheng, et al., Appl. Catal. B: Environ. 272 (2020) 119006.
[33] X. Chen, Q. Li, J. Li, J. Chen, H. Jia, Appl. Catal. B: Environ. 270 (2020) 118915.
[34] X. Li, C. Tung, L. Wu, Nat. Rev. Chem. 2 (2018) 160–173.
[35] J. Du, Z. Du, J.-S. Hu, et al., J. Am. Chem. Soc. 138 (2016) 4201–4209.
[36] X. Zeng, T. Zhou, C. Leng, et al., J. Mater. Chem. A 2 (2017) 17499–17505.
[37] J. Fu, B. Zhu, C. Jiang, et al., Small 13 (2017) 1603938.
[38] Q. Gao, P. Chen, Y. Zhang, Y. Tang, Adv. Mater. 20 (2008) 1837.
[39] F. Yu, L. Wang, Q. Xing, et al., Chin. Chem. Lett. 31 (2020) 1648–1653.
[40] X. Hu, Q. Ji, J.P. Hill, K. Ariga, CrystEngComm 13 (2011) 2237–2241.
[41] X. Wu, Y. Yu, Y. Liu, et al., Angew. Chem. Int. Ed. 51 (2012) 3211–3215.
[42] B. Li, L. Sun, J. Bian, et al., Appl. Catal. B: Environ. 270 (2020) 118849.
[43] A. Li, Q. Cao, G. Zhou, et al., Angew. Chem. Int. Ed. 58 (2019) 14549–14555.
[44] B. Su, L. Huang, Z. Xiong, et al., J. Mater. Chem. A 7 (2019) 26877–26883.
[45] H. Yang, D. Yang, X. Wang, Angew. Chem. Int. Ed. 59 (2020) 15527–15531.
[46] Z. Pan, H. Rao, I. Mora-Sero, J. Bisquert, X. Zhong, Chem. Soc. Rev. 47 (2018) 7659–7702.
[47] W. Xing, X. Zhang, C. Geng, et al., Nanoscale 11 (2019) 8475–8484.
[48] D. Xu, B. Cheng, W. Wang, C. Jiang, J. Yu, Appl. Catal. B: Environ 231 (2018) 368–380.
[49] P.P. Wang, H.Y. Li, H. Liu, et al., Small 11 (2015) 3909.
[50] Y.H. Huang, K. Wang, T. Guo, et al., Appl. Catal. B: Environ 277 (2020) 119232.
[51] F. Li, G.H. Gu, C. Choi, et al., Appl. Catal. B: Environ 277 (2020) 119241.